Nuclear Engineering and Technology 57 (2025) 103585

Contents lists available at ScienceDirect

Nuclear Engineering and Technology

journal homepage: www.elsevier.com/locate/net

Original Article

RUCAS: Software for assessing radiological risk to the public in metallic radioactive waste recycling from decommissioning nuclear facilities

Ugyu Jeong [a], Hyeongjin Byeon [a,b], Jaeyeong Park [a,*]

[a] School of Nuclear Engineering, Ulsan National Institute of Science and Technology, 50 UNIST-gil, Ulsan, 44919, Republic of Korea
[b] Korea Atomic Energy Research Institute, 989-111 Daedeok-daero, Yuseong-gu, Daejeon, 34057, Republic of Korea

ARTICLE INFO

Keywords:
Assessment framework
Decommissioning
Recycling
Radiation protection
Safe disposal
Dose evaluation software

ABSTRACT

Deregulation of the resultant radioactive waste from the increasing decommissioning of nuclear facilities worldwide has become crucial for accurately estimating potential radiological risks to the public. This study introduces the Recycling-Underlying Computational Dose Assessment Software (RUCAS), developed by the Ulsan National Institute of Science and Technology (UNIST) in the Republic of Korea. RUCAS addresses the limitations of existing tools, such as RESRAD-RECYCLE and MicroShield® (MS), which suffer from outdated methodologies and inefficient risk assessments, respectively, while integrating their strengths. By incorporating the latest data, including dose conversion factors and nuclide data, as well as employing the point-kernel method, RUCAS offers a more accurate, robust, and versatile dose assessment framework compared to currently available tools. The advancements made with RUCAS signify substantial progress in developing safer and more feasible recycling strategies for radioactive waste.

1. Introduction

The growing global inventory of nuclear facilities requiring decommissioning has prompted active research to manage the resultant radioactive waste [1–6]. The International Atomic Energy Agency (IAEA) reports that 204 reactors have been permanently shut down, and 154 reactors are currently undergoing decommissioning, with these numbers steadily increasing [7]. A single pressurized water reactor, with a capacity of 900–1300 MWe, can generate 6200 tons of radioactive waste upon decommissioning [8]. Waste management of this nature and capacity transcends sheer volume handling to include addressing the substantial decommissioning costs, which can run into tens of millions of dollars. Among the waste, metallic radioactive materials characterized by low levels of radioactivity amount to 4150 tons, representing 67 % of the total decommissioning waste [9]. These materials, classified as very-low-level waste (VLLW), hold economic value owing to their potential for recycling and reusability. Implementing clearance or deregulation strategies for recycling metallic VLLW mitigates the volume of decommissioning waste and enhances the efficiency of existing disposal facilities.

The IAEA classifies waste with an estimated radiological risk of under 10 μSv per year, in expected post-clearance scenarios, as exempt waste [10], which is acceptable for unrestricted use in various ways, including reuse, recycling, and landfill. In recycling, workers and consumers of recycled-content products are at high risk of exposure to radioactive sources through direct handling or absorption of emitted particulates through respiration or ingestion. Therefore, scenarios considering various recycling situations should be established to ensure the safe clearance or deregulation of radioactive waste, and the radiation risks associated with these scenarios should be accurately assessed. In response, international organizations, including the IAEA, the US Nuclear Regulatory Commission, and the European Commission, have advocated for specific recycling scenarios for radioactive waste [11–14]. Nonetheless, the disparity in assessment methodologies and data among these organizations introduces significant uncertainty regarding radiological risks. This emphasizes the need to develop advanced risk assessment software that integrates and validates diverse recycling scenarios, thereby enhancing radiation protection and optimizing decommissioning costs.

RESRAD-RECYCLE is the conventional dose assessment software for

Abbreviations: DCF, dose conversion factor; FO, furnace operator; PK, point-kernel; RUCAS, Recycling-Underlying Computational Dose Assessment Software; RW, refinery worker; SL, smelter loader; SW, scrap yard worker; VLLW, very-low-level waste.

* Corresponding author.
E-mail address: jypark@unist.ac.kr (J. Park).

https://doi.org/10.1016/j.net.2025.103585
Received 8 December 2024; Received in revised form 24 February 2025; Accepted 13 March 2025
Available online 14 March 2025
1738-5733/© 2025 Korean Nuclear Society, Published by Elsevier Korea LLC. All rights are reserved, including those for text and data mining, AI training, and similar technologies. This is an open access article under the CC BY-NC-ND license (http://creativecommons.org/licenses/by-nc-nd/4.0/).

recycling radioactive scrap, developed by Argonne National Laboratory (ANL) [15]. However, since its last update in 2005, crucial components such as recycling scenarios, dose assessment methodologies, and libraries have not been maintained [16–18]. A notable limitation of RESRAD-RECYCLE is its sole focus on cylindrical source geometry recycling scenarios, which fails to account for varied geometric configurations, potentially compromising the accuracy and reliability of dose assessments in real-world recycling processes. Currently, tools such as MicroShield® (MS) and VISIPLAN 3D ALARA (VISIPLAN) are also utilized for dose assessment in recycling scenarios [5,19]. However, they are limited to evaluating only the external radiation dose associated with a specific scenario [20,21]. This limitation implies that MS and VISIPLAN are unsuitable for a comprehensive risk assessment of recycling flows, necessitating the consideration of multiple pathways, external and internal radiation, and variability of source phase throughout the process. Therefore, advanced software that can accurately assess the transformation flow of scrap through the recycling process is crucial.

The Recycling-Underlying Computational Dose Assessment Software (RUCAS) was developed by the Ulsan National Institute of Science and Technology (UNIST) in the Republic of Korea to overcome the limitations of the existing dose assessment tools for recycling scenarios. It offers a comprehensive evaluation of radiological risks throughout the recycling process, from the generation of radioactive scrap to the final use of the end products. This software incorporates the latest data, methodologies, and recycling scenarios to provide a robust assessment framework [22–24]. This study presents benchmarks designed to validate the enhanced dose assessment capabilities of RUCAS and compares its performance with those of conventional tools. Notably, RUCAS achieved greater accuracy in calculating the shielding effect than RESRAD-RECYCLE. Additionally, comparisons with MS confirmed that RUCAS successfully integrates the latest dose assessment methodology. The validation of these advancements positions RUCAS as a leading tool in the field, setting a new standard for recycling radioactive scrap. The enhanced features of RUCAS are expected to significantly contribute to developing safer and more effective recycling plans for radioactive waste generated during decommissioning.

2. Methods

2.1. Algorithm of RUCAS

Fig. 1 illustrates the detailed dose assessment algorithm used by RUCAS, which operates through dynamic interactions between its calculation modules—concentration, sampling, and dose calculation. These modules utilize a comprehensive database to compute radiation doses effectively. During the data processing phase, RUCAS initially constructs detailed databases that encompass essential radionuclide data along with scenario-specific parameters necessary for accurate dose assessment. Users can create a single input file that includes numerous editable scenarios, as depicted in Fig. 2. The input file is then processed; thus, relevant database information is sorted and transmitted to the appropriate calculation modules tailored for each specific recycling scenario. These calculation modules systemically process the incoming data, derive the results based on the predefined algorithms, and document these results in an output file. This iterative process—encompassing data processing, calculation, and recording—ensures that each recycling scenario selected by the user is evaluated comprehensively.

2.1.1. Concentration module

The scrap metal is transformed into byproducts, specifically ingots, slag, and dust. The concentration module calculates the radioactive concentration of each radionuclide in the recycling process by considering radioactive decay. The radionuclide concentrations are integrated over one year, as shown in Eq. (1), based on the recycling scenario in RUCAS, which considers the activities and product usage during the initial year of the conservative assessment.

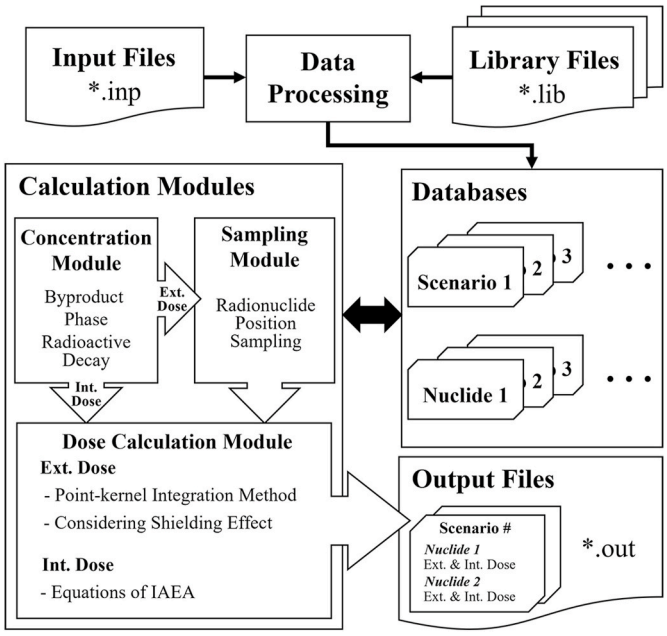

Fig. 1. Comprehensive dose assessment algorithm of Recycling-Underlying Computational Dose Assessment Software (RUCAS).

$$C_{i,1\ year} = \int_0^{1\ yr} C_{i,0} e^{-\lambda t}\, dt = C_{i,0}\left(\frac{1-e^{-\lambda}}{\lambda}\right), \tag{1}$$

where $C_{i,1\ year}$ is the cumulative radioactive concentration of radionuclide i over one year of radioactive decay (Bq/g).

Based on the principles of secular equilibrium and Bateman's equation [25], the radioactive concentration of the progeny resulting from the decay of the parent radionuclide can be derived as follows:

$$C_2(t) = C_1(0)\lambda_2 \frac{(e^{-\lambda_1 t} - e^{-\lambda_2 t})B_2}{\lambda_2 - \lambda_1}, \tag{2}$$

where 1 and 2 denote the parent radionuclide and progeny, respectively, $C(t)$ denotes the radioactive concentration (Bq/g), λ is the decay constant (yr^{-1}), and B is the branching ratio, which denotes the partitioning ratio from the parent to progeny radionuclides.

The maximum time t_{max} (yr) can be derived from the derivative of the progeny concentration $C_2(t)$ as follows:

$$t_{max} = \frac{log\ (\lambda_2/\lambda_1)}{\lambda_2 - \lambda_1}. \tag{3}$$

In converting scrap metal into byproducts, such as ingots, slag, and dust, the radioactive concentrations of these byproducts, $C_{i,byproduct,1year}$ (Bq/g), within the recycling flow can be expressed as the product of the mass and radionuclide partitioning factors, as illustrated in Eq. (4).

$$C_{i,byproduct,1\ year} = C_{i,1\ year} \times RPF_{i,byproduct} \times \frac{W_{scrap}}{MPF_{byproduct}}, \tag{4}$$

where $RPF_{i,byproduct}$ denotes the radionuclide partitioning factor for radionuclide i, indicating the radioactivity ratio of the byproduct to the total radioactivity, W_{scrap} denotes the dilution factor, the fraction of the contaminated scrap metal in the total waste, and $MPF_{byproduct}$ is the mass partitioning factor for the byproduct, which is the ratio of the byproduct mass to the total mass.

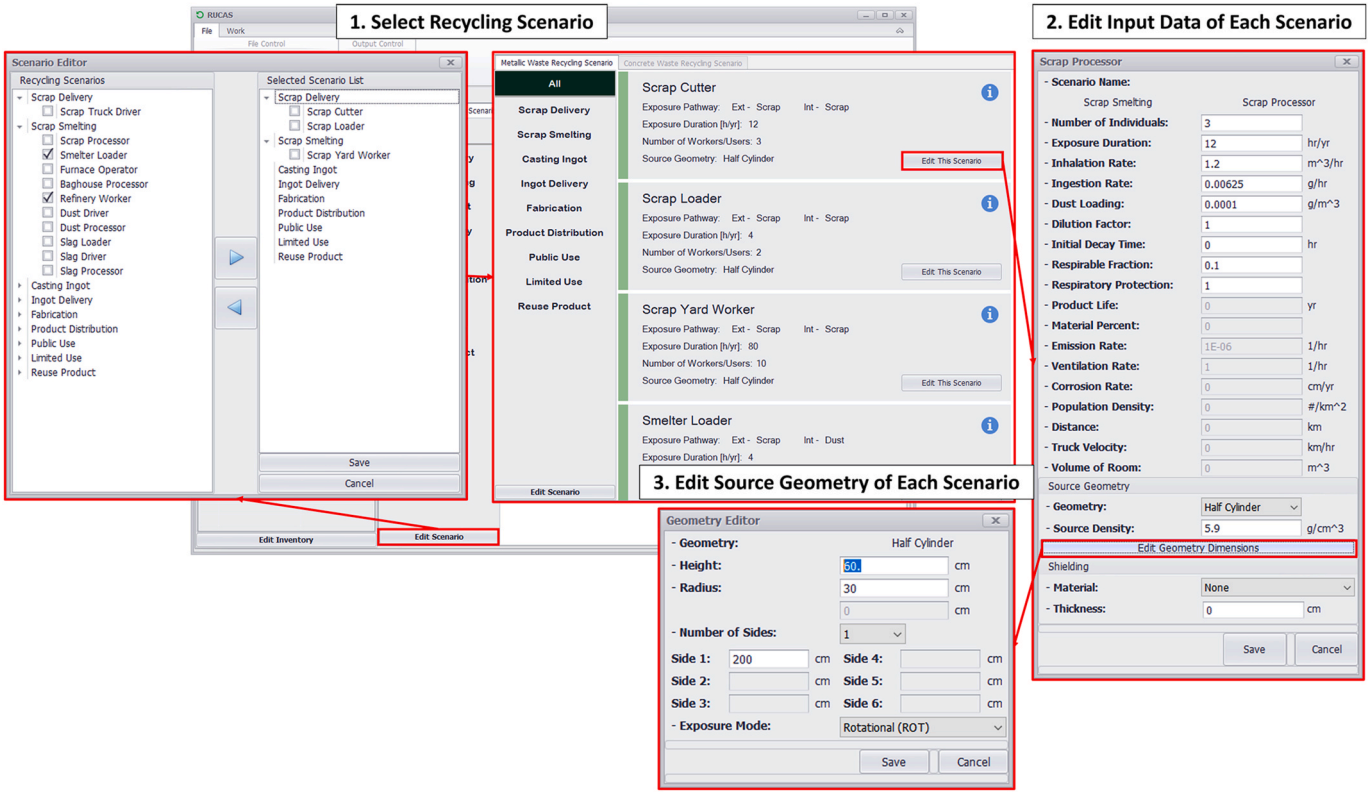

Fig. 2. Interface of the scenario editor in RUCAS.

2.1.2. Sampling module

The point-kernel (PK) method is used within RUCAS to evaluate various source geometries in external dose assessments [26], and it requires uniformly sampling numerous point sources within a specified volumetric source geometry. This improves the risk assessment performance by simulating realistic radioactive source forms, such as drums, stacked piles, and buildings, using the geometries supported by RUCAS, as detailed in Table 1. As shown in Fig. 3, when the geometric dimensions of a volumetric source are provided, point sources are uniformly sampled using the acceptance-rejection rule and Latin hypercube sampling methodology [27]. In Fig. 3, the light and dark regions represent unit volumetric sources and volumetric sources based on the input values, respectively. Given the shape and volume of the source as input values, the process involves forming a unit volumetric source with all dimensions set to 1 and then sampling the point sources within it. Subsequently, the coordinates for each point source are expanded based on the input dimensions—radius, height, width, and depth—to derive the final coordinates of the point sources.

2.1.3. Dose calculation module

The dose calculation module receives the radionuclide-specific radioactive concentrations and coordinates of the point sources from the concentration and sampling modules, respectively. It then calculates the doses from three exposure pathways: external, inhalation, and ingestion. For the internal dose, the dose assessment model of the IAEA, subsuming inhalation and ingestion exposures, was incorporated into RUCAS by using the following equations [28].

$$H_{INH} = T \times IH \times DL \times PF \times RF \times \sum_i \left(C_{i,1\ year} \times DCF_{INH,i}\right), \tag{5}$$

$$H_{ING} = T \times \sum_i \left(C_{i,1\ year} \times DCF_{ING,i}\right) \times [IH \times DL \times PF \times (1 - RF) + IG], \tag{6}$$

where the subscripts *INH* and *ING* represent the exposure pathways of inhalation and ingestion, respectively, H denotes the annual effective dose equivalent (Sv/yr), T is the annual exposure duration (h/yr), IH is the inhalation rate (m^3/h), IG is the ingestion rate (g/h), DL represents the dust loading in the air (g/m^3), PF denotes the respiratory protection afforded by personal protective equipment, RF is the respirable fraction, and DCF represents the dose conversion factor (DCF) of radionuclide i (Sv/Bq).

For the external dose, the annual effective dose equivalent H can be expressed as the product of the total radioactivity of radionuclide i at the source, dose rate for radionuclide i, DR_i (Sv/h), and exposure duration T, as shown in the following equation:

$$H_{ext} = \sum_i C_{i,1\ year} \times M_{source} \times DR_i \times T, \tag{7}$$

where M_{source} is the total mass of the radioactive source. The dose rate for radionuclide i, DR_i can be expressed as the product of the annual photon flux from the gamma energy group, ϕ_E ($cm^{-2} \bullet yr^{-1}$), and the flux-dose conversion coefficient by the gamma energy group, h_E ($Sv \bullet cm^2$) [23, 29]. According to the PK method, the sum of the flux from each point source can be derived by separating the volumetric source into numerous point sources, as follows [26]:

$$DR = \sum_E h_E \phi_E, \tag{8}$$

Table 1
Source geometries supported in RUCAS.

Cylinder	Sphere
Half cylinder	Annular cylinder
Disk	Half disk
Line	Half sphere
Rectangular volume	Plane

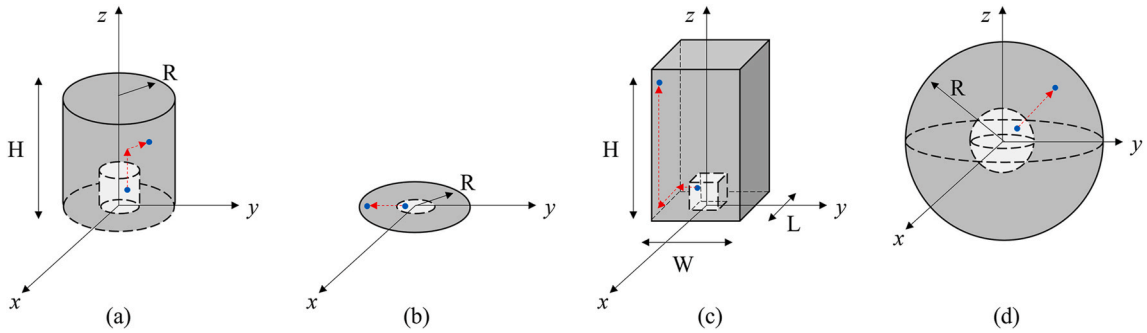

Fig. 3. Source sampling method for source geometry of (a) cylinder, (b) disk, (c) rectangular volume, and (d) sphere.

$$\phi_E = \sum_{s=1}^{N} \frac{W_E B_{E,s} e^{-\mu_E \tau_s}}{4\pi\rho_s^2 N}, \tag{9}$$

where W_E is the photon yield for the gamma energy group E [23,30], $B_{E,s}$ is the buildup factor of the photon s within the gamma energy group E, and μ_E is the linear attenuation coefficient for the gamma energy group E (cm^{-1}), determined as the product of the mass attenuation coefficient and density of the medium [31]. Additionally, τ_s is the straight-line distance traveled by photons generated from the point source s (cm), ρ_s denotes the distance between the point source s and a receiver, and N is the total number of sampled sources.

RUCAS accounts for the attenuation of radiation through various media by expressing the shielding effect as the buildup factor B_E. According to geometric progression fitting, it can be expressed as Eqs. (10) and (11) [32].

$$B_{E,s} = \begin{cases} 1 + (b-1)\dfrac{K^{x_{E,s}} - 1}{K - 1}, K \neq 1 \\ 1 + (b-1)x_{E,s}, K = 1 \end{cases}, \tag{10}$$

$$K = cx_{E,s}^{a} + d\frac{\tanh\left(\frac{x_{E,s}}{\xi_k - 2}\right) - \tanh(-2)}{1 - \tanh(-2)}. \tag{11}$$

Here, $b, c, a, d,$ and ξ_k are the buildup factor coefficients and $x_{E,s}$ is the number of mean free paths (mpf), calculated as the product of the linear attenuation coefficient μ_E for the gamma energy group E and the distance τ_s traveled by photons emitted from the point source s.

To account for the shielding effect in multiple media, both methods are used to derive the total buildup factor from the buildup factors of the shielding and source addressed in prior studies [33,34]. The total buildup factor of multilayer shielding can be expressed as the following equations:

$$\begin{aligned} B_{tot}(x_1, x_2) &= B_2(x_2) + [B_2(x_1 + x_2) - B_2(x_2)][K(x_1)C(x_2)] \\ K(x_1) &= \frac{B_1(x_1) - 1}{B_2(x_1) - 1} \end{aligned}, \tag{12}$$

where the subscripts 1 and 2 denote the source and shielding, respectively; B_{tot} is the total buildup factor; and the buildup factors of the source B_1 and shielding B_2 can be derived from Eq. (10). $C(x_2)$ is based on the methods proposed by Kalos [33] and Lin and Jiang [34] and can be represented by Eqs. (13) and (14), where μ_c represents the linear attenuation coefficient of Compton scattering, μ_t is the total linear attenuation coefficient, and Z is the atomic number.

$$C(x_2) = \begin{cases} 1 \; when \; Z_1 > Z_2 \\ exp(-1.7x_2) + \dfrac{\alpha}{K(x_1)}[1 - exp(-x_2)] \; when \; Z_1 < Z_2 \end{cases}, \tag{13}$$

$$\alpha = \frac{(\mu_c/\mu_t)_1}{(\mu_c/\mu_t)_2}$$

$$C(x_2) = \begin{cases} exp(-1.08\beta x_2) + 1.13\beta l(x_2) \; when \; Z_1 > Z_2 \\ 0.08l(x_2) + \dfrac{\gamma}{K(x_1)} exp(-x_2) \; when \; Z_1 < Z_2 \end{cases}. \tag{14}$$

$$\beta = \frac{(\mu_t/\rho)_2}{(\mu_t/\rho)_1}, \gamma = \frac{(\mu_c/\rho)_1}{(\mu_c/\rho)_2}, l(x_2) = \frac{B_2(x_2) + 1}{B_1(x_1) + 1}[1 - exp(-x_2)]$$

2.1.4. Recycling scenario

RUCAS assumes a comprehensive range of recycling scenarios for metallic radioactive waste, from its generation to the use of the final product [11–14]. As depicted in Fig. 4, the recycling process is divided into seven steps: (1) scrap delivery, (2) scrap smelting, (3) casting ingot, (4) ingot delivery, (5) product fabrication, (6) product distribution, and (7) product end use. During the initial six steps, the potential exposure to workers, such as loaders, drivers, processing facility workers, and foundry workers, is considered. In the product end-use step, the potential exposure is assumed to arise from the use of the final product, such as parking lots, home/office buildings, furniture, and appliances produced from the byproducts generated from the recycling process. Thus, RUCAS comprises 55 recycling scenarios targeting both workers and product users to evaluate the radiological risk arising from radioactive scrap recycling.

3. Benchmarking of dose assessment software

In this study, several benchmarks of RUCAS were used with RESRAD-RECYCLE and MS to validate its capability for the risk assessment of contaminated scrap metal recycling. Notwithstanding its lack of updates and maintenance, RESRAD-RECYCLE was selected first for comparison because it reflects the overall recycling flow of metallic radioactive waste, and the dose assessment methodology for internal exposure has remained largely unchanged. Owing to the incompatibility of RESRAD-RECYCLE with modern computer operating systems, the results of a validation conducted by the Swedish Radiation Protection Authority (SSI) using RESRAD-RECYCLE were referenced in this study [35]. However, because RUCAS applies an updated external dose assessment model, relying solely on RESRAD-RECYCLE for validation does not adequately confirm the reliability of the external dose assessment model. MS, which is consistently used for external dose and shielding effect assessments, was also selected for comparison to further ensure the reliability and evaluate the additional functionalities of RUCAS.

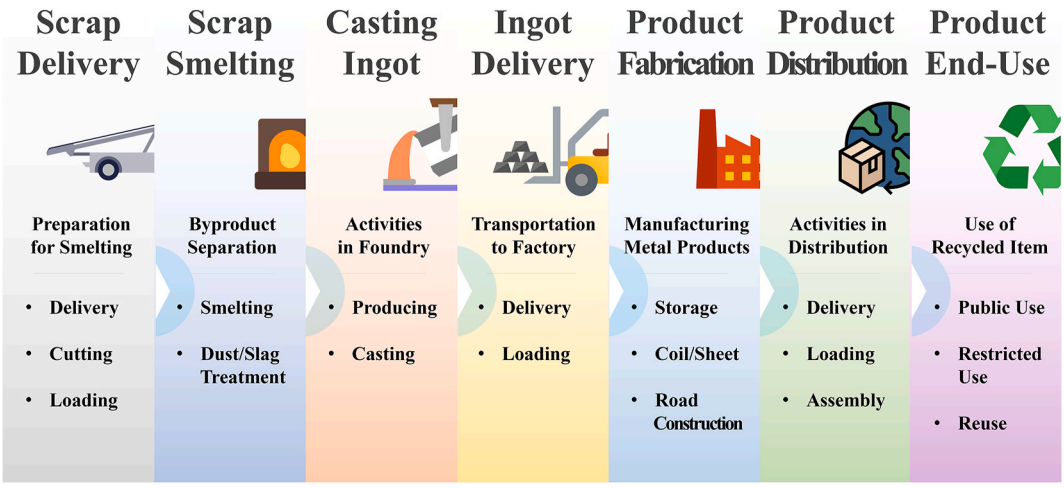

Fig. 4. Recycling steps for metallic radioactive waste in RUCAS.

3.1. Benchmarking for recycling scenarios

The first benchmark addresses the validation of the multi-scenario calculation capability of RUCAS. Table 2 shows the conditions used for the benchmark, with RUCAS and RESRAD-RECYCLE utilizing the built-in scenarios for evaluation. Because MS does not support scenario evaluation, it replicates the exposure models for each scenario (Table 2) and performs iterative calculations. The recycling scenarios considered the melting of stainless steel from the structural components of nuclear fuel assemblies at the Swedish nuclear power plant and were divided into six scenarios [35]. The scenarios were based on the actual proximity of the workers to the source, the duration of their work, and the measured concentrations of radionuclides at the time of processing. The radionuclides considered for dose assessment included Co-60, Sb-125, Cs-134, Cs-137, and Eu-154.

3.2. Benchmarking for shielding effect

This study utilized another benchmark for the shielding effect calculation capabilities of RUCAS by shielding the scenarios suggested in the RESRAD-RECYCLE validation report [35]. A 30-cm concrete shielding was included owing to the default recycling scenarios of RESRAD-RECYCLE. The scenarios used for benchmarking, detailed in Table 3, cover various stages of the operations at the smelters. These scenarios represent a distinct, multilayered configuration in which the source and shielding materials differ significantly. The methodology proposed by Lin and Jiang [34] in Eq. (14) was applied to RUCAS for this benchmarking. The dose assessment considered radionuclides at a concentration of 1 Bq/g, including Ac-227, Am-241, Co-60, Cs-137, Pu-239, U-238, and Zn-65 [35]. The mass partitioning factors were 90 % for the ingots, 10 % for the slag, and 1 % for the dust [11,36,37]. The radionuclide partitioning factors are used according to previous researches [11,37,38].

Table 3
Benchmarking conditions for recycling scenarios with 30 cm of concrete shielding.

Calculation parameter	Scrap yard worker	Smelter loader	Furnace operator	Refinery worker
Source geometry	Half Cylinder	Half Cylinder	Cylinder	Cylinder
Shielding effect	O	O	O	O
Shielding material	Concrete	Concrete	Concrete	Concrete
Shielding thickness (cm)	30	30	30	30
Shielding density (g/cm^3)	2.8	2.8	2.8	2.8
Mass (t)	3	3	3	3
Source density (g/cm^3)	5.9	5.9	7.86	7.86
Source height (cm)	109	109	79	73
Radius (cm)	54	54	40	41
Distance (cm)	1000	400	300	300
Exposure duration (h/yr)	24	1.2	1.5	1.5

3.3. Benchmarking for source geometry

The final benchmarking was used to verify the enhanced functionalities of RUCAS related to external dose assessment in realistic radiation scenarios using various comparable geometries and shielding. Specifically, the study evaluated the doses for five source geometries: (1) cylinder, (2) disk, (3) plane, (4) rectangular volume, and (5) sphere with

Table 2
Recycling scenarios for melting stainless steel from nuclear fuel assemblies at a Swedish nuclear power plant.

Calculation parameter	Scrap truck driver	Scrap loader	Scrap cutter	Ingot caster	Ingot truck driver	Slag worker
Source geometry	cylinder	cylinder	cylinder	cylinder	cylinder	cylinder
Shielding effect	O	X	X	O	X	O
Shielding material	Iron	–	–	Iron	–	Iron
Shielding thickness (cm)	0.3	0	0	8	0	1.2
Shielding density (g/cm^3)	7.86	0	0	7.86	0	7.86
Mass (t)	3.3	3	3.3	3.2	3.2	0.006
Source density (g/cm^3)	0.13	0.13	0.13	7.86	7.86	1.5
Source height (cm)	400	400	400	100	250	20
Radius (cm)	145	145	145	40	23	25
Distance (cm)	150	50	30	100	200	50
Exposure duration (h/yr)	0.15	3.7	9.95	0.7	0.2	0.2

concrete medium shielding. The evaluation considered eleven radionuclides that are prominent in decommissioning waste and are known to emit high-energy photons, according to the IAEA [39]. These include Co-60, Mn-54, Cs-137, Sb-125, Eu-152, and Eu-154 as gamma emitters dominant in decommissioning waste, and Zn-65, Ru-106, Ag-110m, and Ce-144 as additional gamma emitters at a concentration of 1 Bq/g. For radioactive sources, it was assumed that a 30 cm-thick concrete barrier shielded 10 tons of scrap metal, and workers were positioned 200 cm away from the source. Table 4 presents the exposure scenario conditions used in the benchmarking. In this benchmarking, RUCAS utilized both formulas of the multilayer buildup factor in Eqs. (13) and (14) [33,34], allowing for a comparative analysis of these methodologies.

4. Results

4.1. Benchmarking results for recycling scenarios

For the six scenarios in this study involving the melting of stainless steel structures from nuclear fuel assemblies, Table 5 presents the average dose ratios for both the internal and external exposure pathways across radionuclides in the recycling scenarios. As presented in Table 5, the internal dose results for RUCAS matched those of RESRAD-RECYCLE. For external exposure doses, both the RESRAD-RECYCLE and MS results were similar to those of RUCAS, with MS results exhibiting slightly greater similarity. The scenarios were categorized based on shielding to facilitate a more detailed analysis from multiple perspectives. The non-shielding scenarios comprised three elements: scrap loader, scrap cutter, and ingot truck driver, whereas the shielding scenarios included scrap truck driver, ingot caster, and slag worker.

Fig. 5 illustrates the comparison of the external exposure dose ratios for different radionuclides between the shielding and non-shielding scenarios. In the three non-shielding scenarios, the results were quantified using the average comparison ratios. The average comparison ratios between RUCAS and MS exhibited a consistent trend across all three scenarios. The ratios of RESRAD-RECYCLE varied between 0.96 and 1.18, indicating some differences, whereas those of MS were close to 1.00. Both comparisons demonstrate considerably low standard deviations for all radionuclides.

In the shielding scenarios, the results of RUCAS were similar to those of MS, which is consistent with the findings for the non-shielding scenarios. However, when compared with the results of RESRAD-RECYCLE, RUCAS displayed significant differences for radionuclides, such as Co-60 and Sb-125, in the ingot caster scenario, which utilized the thickest shielding of 8 cm, showing a ratio of 3.11. Notably, radionuclides such as Cs-134, Cs-137, and Eu-154 were not considered in this scenario because they were not converted into ingots during the recycling process, according to the radionuclide partitioning factors [35]. Furthermore, scenarios involving thinner shields showed dose ratios similar to those in the non-shielding scenarios; however, as the shielding thickness increased, a decreasing trend in external dose ratios across the radionuclides was observed.

Table 4
Benchmarking conditions for various cylinder, disk, plane, rectangular volume, and sphere source geometries.

Source[a] geometry	Source thickness [cm]	Dimension[b] [cm]	Distance [cm]	Shielding[c] thickness [cm]
Cylinder	100	63.88	200	30
Disk	0	63.88	200	30
Plane	0	112.79/ 112.79	200	30
Rectangular volume	100	112.79/ 112.79	200	30
Sphere	0	67.22	200	30

[a] Source material is 7.86 g/cm^3 of iron.
[b] In cylindrical geometries, the radius is used, while in rectangular and planar geometries, the dimensions are specified by width and height.
[c] Shielding material is 2.8 g/cm^{3}of concrete.

Table 5
Average dose ratios of internal and external exposure pathways calculated from the data of five radionuclides measured in the recycling scenario of melting stainless steel from nuclear fuel assemblies at a Swedish nuclear power plant.

#	Recycling scenario	Average ratio for external dose		Average ratio for internal dose
		RUCAS/ RESRAD	RUCAS/ MicroShield®	RUCAS/RESRAD
1	Scrap truck driver	1.03	1.01	1.00
2	Scrap loader	1.06	1.00	1.00
3	Scrap cutter	1.06	1.00	1.00
4	Ingot caster	3.11	1.02	1.00
5	Ingot truck driver	1.07	1.01	1.00
6	Slag worker	0.98	1.01	1.00

4.2. Benchmarking results for shielding scenarios

The analysis was separated according to the radionuclide group, specifically alpha (Ac-227, Am-241, Pu-239, and U-238) and gamma (Co-60, Cs-137, and Zn-65) emitters. Tables 6 and 7 present the average dose ratios for both the alpha and gamma radionuclide groups across the four scenarios. For internal exposure doses, the comparison between RUCAS and RESRAD-RECYCLE showed matching dose ratios of 1.00 for both the alpha and gamma groups, indicating precise agreement between their calculation results, as in the previous benchmarking results. For external dose ratios, the alpha radionuclides exhibited dose ratios ranging from 1.07 to 1.14 between RUCAS and MS, whereas the comparison between RUCAS and RESRAD-RECYCLE displayed much broader dose ratios ranging from 2.88E+08 to 1.56E+08. For the gamma radionuclides, the RUCAS results, when compared with the MS results, showed dose ratios ranging from 1.06 to 1.11, whereas a range of 5.80–6.36 was observed when compared with the RESRAD-RECYCLE results. Given that the internal exposure doses are predominant for alpha radionuclides, this analysis focused on gamma radionuclides to provide a detailed assessment of their external dose ratios.

Fig. 6 shows the characteristics and corresponding external dose ratios of the shielding scenarios—scrap yard worker (SW), smelter loader (SL), furnace operator (FO), and refinery worker (RW). Unlike earlier comparisons, discrepancies were observed between RUCAS and MS, notably with the Cs-137 radionuclide in FO, showing a ratio of 1.2. The difference between RUCAS and RESRAD-RECYCLE was more pronounced under the concrete-shielding condition.

RESRAD-RECYCLE and MS showed similar trends across scenarios. As depicted in Fig. 6, the FO and RW scenarios produced nearly identical ratios under identical source density and exposure distance conditions, as represented by a straight line in the graph. However, variations in the source density and exposure distance led to different dose ratios, indicating a tendency for these ratios to change proportionally with the source density and exposure distance, with the former having a more significant effect than the latter. Furthermore, the extent of these changes varied based on radionuclide, with Cs-137 exhibiting the most significant variation, followed by Zn-65 and Co-60, which showed smaller changes.

4.3. Benchmarking results of source geometries

For the five source geometries featuring an iron source and concrete shielding, the external doses from different radionuclides varied significantly based on the calculation conditions. Consequently, the results are presented as ratios between the outcomes obtained from RUCAS and

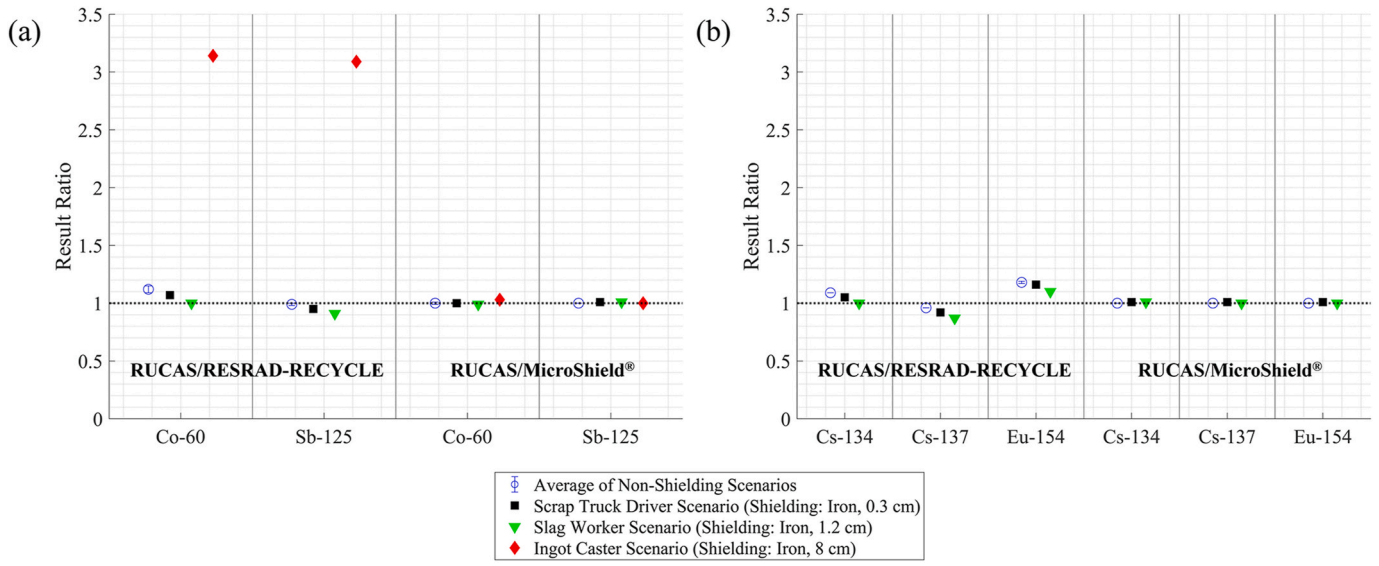

Fig. 5. External dose ratios of shielding and non-shielding scenarios for radionuclides (a) existing in both slag and ingot forms, such as Co-60 and Cs-137; and (b) existing only in slag form, such as Cs-134, Cs-137, and Eu-154.

Table 6
Average external and internal dose ratios for alpha emitters across recycling scenarios with 30 cm of concrete shielding.

Alpha emitters	Average ratio for external dose		Average ratio for internal dose
	RUCAS/RESRAD	RUCAS/MicroShield®	RUCAS/RESRAD
Ac-227	2.88E+01	1.14	1.00
Am-241	1.56E+08	1.12	1.00
Pu-239	3.23E+02	1.16	1.00
U-238	1.10E+02	1.07	1.00

Table 7
Average external and internal dose ratios for gamma emitters across recycling scenarios with 30 cm of concrete shielding.

Gamma emitters	Average ratio for external dose		Average ratio for internal dose
	RUCAS/RESRAD	RUCAS/MicroShield®	RUCAS/RESRAD
Co-60	6.36	1.06	1.00
Cs-137	6.08	1.11	1.00
Zn-65	5.80	1.08	1.00

those from MS. Table 8 displays the average result ratios between RUCAS and MS. For the multilayer shielding in RUCAS, these ratios were calculated by applying two different buildup factor calculation methodologies proposed by Kalos [33] and Lin and Jiang [34].

The external dose assessments for gamma radionuclides for the five different geometries showed that when the methodology of Kalos (1956) was applied to RUCAS, the result ratios ranged from 1.02 to 1.04, closely matching those of MS. When using the Lin and Jiang [34] (LJ) methodology, the result ratios ranged from 1.04 to 1.14, which were similar to those of MS but showed higher doses than those obtained with Kalos. However, for the disk and plane geometries that considered only the attenuation effects of the shielding medium, the result ratios consistently remained at 1.04, regardless of the methodology used.

Fig. 7 presents the average result ratios across three volumetric geometries: cylinder, rectangular volume, and sphere, considering both the source and shielding attenuation effects. As shown in Fig. 7, the standard deviation in the average result for each radionuclide was

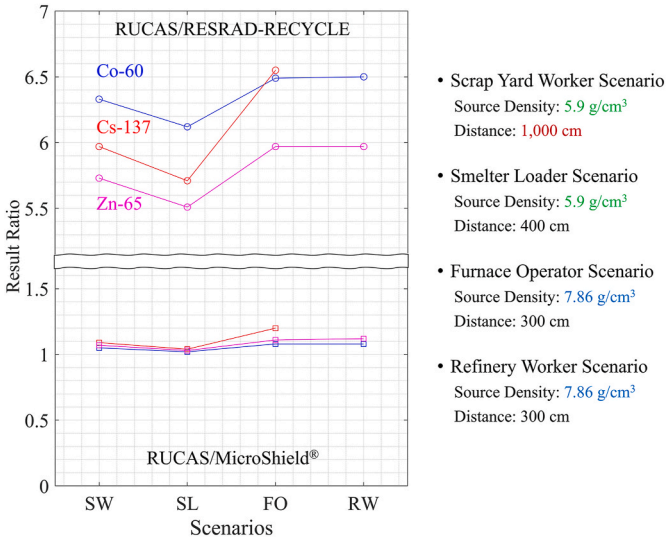

Fig. 6. Characteristics and external exposure dose ratios for different gamma emitters for recycling scenarios with 30 cm of concrete shielding.

Table 8
Average external exposure dose ratios for five source geometries under iron source-concrete-shielding condition, obtained by applying two buildup factor calculation methodologies for multilayer shielding [33,34].

#	Source geometry	RUCAS/MicroShield®	
		Kalos et al. (1956)	Lin and Jiang (1996)
1	Cylinder	1.02	1.13
2	Disk	1.04	1.04
3	Plane	1.04	1.04
4	Rectangular volume	1.02	1.13
5	Sphere	1.03	1.14

diminutive. Moreover, while the methodologies of Kalos and LJ varied in the extent of their differences compared to the MS method, they consistently exhibited the same error direction across all radionuclides. For example, the Kalos and the LJ methods both demonstrated a similar pattern, where the largest discrepancies and an increasing trend in the

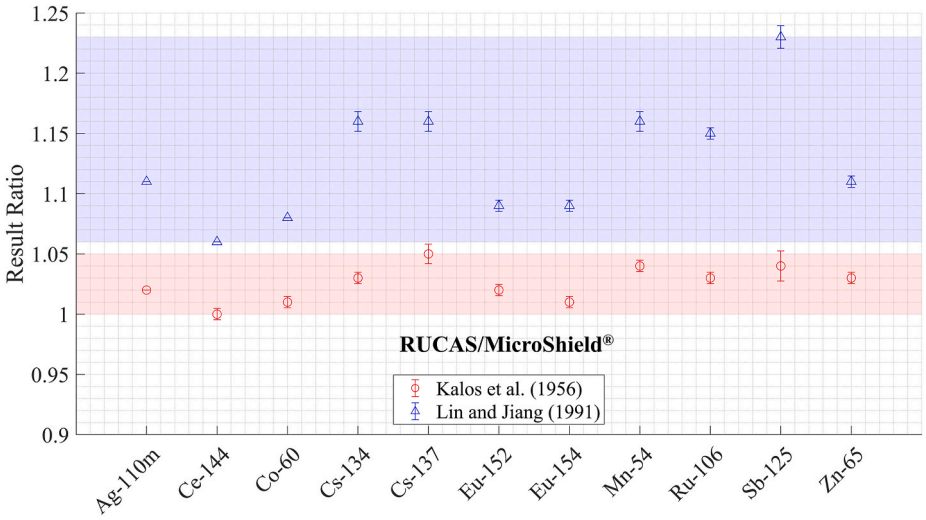

Fig. 7. Average external exposure dose ratios for gamma emitters across five source geometries.

resulting ratios were observed for the radionuclides Cs-137 and Sb-125.

5. Discussion

Benchmarks for various recycling scenarios were used to verify the RUCAS risk assessment model. The comparison included external dose assessments among the three software programs: RUCAS, RESRAD-RECYCLE, and MS, whereas the internal exposure doses were compared between RUCAS and RESRAD-RECYCLE. The internal doses displayed identical values for both RUCAS and RESRAD-RECYCLE, similar to the methodology proposed by the IAEA [28]. For external radiation doses, the presence or absence of shielding altered the trends of the results. In non-shielding scenarios, the results of RUCAS were nearly identical to those of MS and differed slightly from those of RESRAD-RECYCLE. In shielding scenarios, RUCAS showed results similar to those of MS but significantly different from RESRAD-RECYCLE. This difference was exacerbated when the source and shielding materials differed.

Based on previous studies and Eqs. (9)–(14), the dose assessment variations across the codes can be attributed to three primary factors. First, the disparity between the external dose assessment models of RUCAS and RESRAD-RECYCLE was identified as a significant source of variance. RUCAS and MS utilized the latest models based on the PK method, which internally calculates the DCF, whereas RESRAD-RECYCLE applied a fitting approach to the external DCFs from Federal Guidance Report No. 12 [17]. The second reason is assumed to be the differences between the methodologies for calculating the multilayer buildup factors. Various methodologies have been proposed for calculating the buildup factors when the source and shielding materials differ [32–34,40–43], and these methodology variations are understood to cause differences in the external radiation doses [44]. The absence of information regarding the methodology used by MS has led to this assumption. Finally, differences in the attenuation coefficient are believed to influence the dose results. Eqs. (9)–(14) reveal that the attenuation coefficient is pivotal in determining the buildup factor, particularly when the medium is a mixture, leading to significant variations depending on the composition [45–47]. These three reasons explain the variations observed in the benchmark calculations.

5.1. Discussion on benchmark results

In the benchmark for recycling scenarios involving the melting of stainless steel from the structural components of nuclear fuel assemblies at the Swedish nuclear power plant, the difference in the external dose assessment model between RUCAS and RESRAD-RECYCLE was clearly illustrated. The scenarios used in this benchmark involved the same materials for source and shielding, specifically pure iron, leading to the assumption that the effect of differences in attenuation coefficient would be negligible. Additionally, because the effect of the multilayer buildup factor was not considered under this condition, the same external dose assessment model was applied to RUCAS and MS by excluding these influences. As indicated in Table 5, the resulting ratio between RUCAS and MS was nearly identical, ranging from 1.00 to 1.02, whereas that between RUCAS and RESRAD-RECYCLE showed significant differences, increasing to 3.11 as the shielding thickness increased. The similarity between RUCAS and MS results validated the effectiveness of the external dose assessment method applied in RUCAS. Furthermore, the lower doses from RESRAD-RECYCLE, which are perhaps one-third of those estimated by RUCAS under thicker shielding conditions, are considered to potentially affect the reliability of the risk assessment.

In the benchmarking for the shielding recycling scenarios, the effect of the attenuation coefficients on the external dose for each radionuclide was indirectly observed. Differences in the mass attenuation coefficient between the codes for the photon energy groups are expected to correspond to the gamma emission spectra, resulting in variations in the external doses across radionuclides. As indicated in Eq. (10), the number of mean free paths used in the buildup factor calculations can be expressed as the product of the source density, exposure distance, and mass attenuation coefficient. The results shown in Fig. 6 suggest that source density and exposure distance influence the discrepancies between the codes, with Cs-137 (emitting 0.662 MeV of gamma) being more sensitive to changes than Co-60 (1.17 and 1.33 MeV) and Zn-65 (1.12 MeV), which emit similar levels of gamma energies and show similar sensitivity levels. These findings suggest differences in the concrete mass attenuation coefficients of the three software products compared in this study. Given that the discrepancies with RESRAD-RECYCLE were observed to be approximately six times greater under concrete-shielding conditions, the use of RUCAS is more suitable for risk assessment because of its reliability and conservation.

In the benchmarking process for various source geometries, the differences observed between RUCAS and MS were examined to ascertain whether they stemmed solely from variations in the attenuation coefficient or could be attributed to differences in the multilayer buildup factor methodology. In the study by Basu et al. [44], where the thickness of the iron source was three times that of the concrete shielding (3 mean free paths (mfp) of iron followed by 1 mfp of concrete), the LJ method produced a dose that was 1.07 times higher than that obtained with the Kalos method [44]. Consistent with these findings, our study revealed

that the LJ method results were 1.11 times higher than those of the Kalos method, indicating a similar trend that accounts for both the buildup factor methodology and the effects of the attenuation coefficients. Both methodologies produced dose results comparable to those obtained using MS, which confirms the accuracy of the shielding calculations performed by RUCAS. Additionally, the consistent similarities between RUCAS and MS results across different source geometries suggest that the RUCAS sampling module is functionally efficient. These similarities, independent of the source geometry, further verify the effectiveness and reliability of conducting comprehensive and accurate radiological assessments.

Based on the study analyses and observations, several conclusions about the differences in the concrete mass attenuation coefficient between RUCAS and MS have been drawn. First, the dose results for pure iron, a material where differences in the attenuation coefficient are typically unanticipated, were similar for RUCAS and MS. This suggests that both systems calculate radiation attenuation in iron consistently, underscoring the accuracy of both tools in handling materials with well-established properties. (2) As presented in Table 8, for 2D source geometries such as disk and plane, which are expected not to exhibit effects of source medium attenuation, the resulting ratios remain constant at 1.04 for both the Kalos and LJ methodologies. (3) The error sensitivity direction and level across the radionuclides are consistent, irrespective of the multilayer buildup factor calculation methodology applied. Despite these consistent findings, the specific type of concrete used in the MS calculations presented a gap, as MS reportedly utilizes an ANSI/ANS report and NIST data. To address this, the mass attenuation coefficients of three reference concretes, as provided by ANSI/ANS and NIST, were compared [31,48].

For comparative analysis, the mass attenuation coefficients of these reference concretes were applied to RUCAS, considering the presence or absence of coherent scattering. These tests were conducted under benchmark conditions that replicated a 100-cm iron cylindrical source shielded by a 30-cm concrete barrier. Fig. 8 shows the external exposure dose result ratios between RUCAS and MS for the mass attenuation coefficients of the reference concretes. When using the mass attenuation coefficients from ANSI/ANS 6.4.3 NBS Concrete with coherent scattering and NIST Portland concrete with coherent scattering, the RUCAS results are similar to those of MS. This confirms that the differences previously observed between RUCAS and MS results using the Kalos method were attributed to differences in the attenuation coefficient rather than a fundamental issue with applying the methodology.

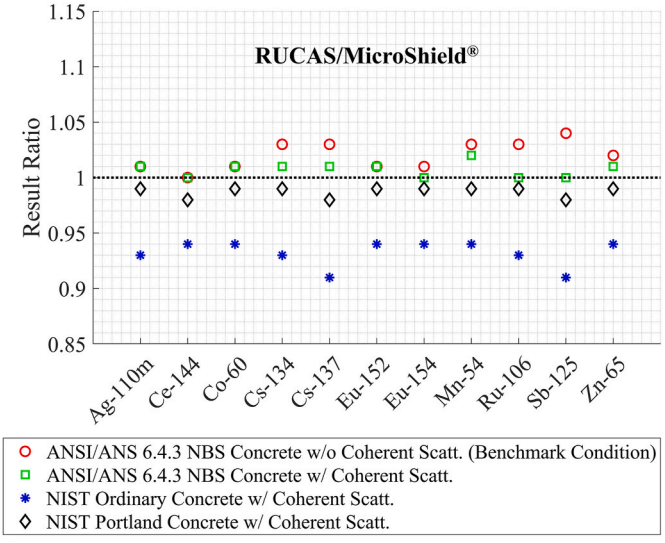

Fig. 8. External radiation dose ratios for the attenuation coefficients of reference concretes.

Moreover, the variation in the dose values depending on the concrete composition underscores the importance of accurate material characterization in radiological assessments.

5.2. Potential and limitations

As shown in Table 9, the analysis of benchmark results shows the merits of RUCAS compared to other conventional dose assessment software, such as MS and RESRAD-RECYCLE. Because the results affirmed the validity of the models employed in RUCAS for assessing external and internal exposure doses to the byproducts: ingots, slag, and dust, which are transformed during the recycling process, RUCAS offers the following benefits:

First, RUCAS demonstrated a more accurate evaluation model for shielding effects and for various source geometries compared to RESRAD-RECYCLE. In multi-layer shielding calculations, the editable attenuation coefficients and enhanced methodology of RUCAS contribute to a synergistic effect, leading to improved calculation accuracy and conservatism, as evidenced by higher dose estimates compared to RESRAD-RECYCLE. These findings suggest that RUCAS has the potential to serve as a replacement for RESRAD-RECYCLE in the safety assessment of radioactive waste recycling, where safety is a critical consideration.

Furthermore, RUCAS can also access multiple exposure scenarios including various exposure pathways such as external exposure, ingestion, and inhalation, in a single calculation while maintaining a level of accuracy comparable to MS in external dose assessment. In contrast, as MS is exclusively designed for external dose evaluation and does not support internal exposure calculations, it requires separate analyses for each recycling scenario and additional internal dose assessment software to conduct a comprehensive safety assessment of decommissioning waste recycling. Conversely, RUCAS simplifies the process by evaluating built-in recycling scenarios in a single calculation, providing a comprehensive analysis of radionuclide partitioning and various exposure pathways. Therefore, RUCAS offers a significant advantage in the safety assessment of decommissioning waste recycling.

However, the effectiveness of RUCAS was validated using recycling scenarios and results from the RESRAD-RECYCLE validation report [35]. The limited range of scenario conditions evaluated prevented a comprehensive analysis of dose result ratios between RESRAD-RECYCLE and RUCAS, particularly in terms of variations in shielding thickness. Additional validations are necessary for product use scenarios, worker scenarios, and other source geometries not included in these

Table 9
Functional comparisons of RUCAS with conventional software in the safety assessment for the recycling of decommissioning waste.

Features	RUCAS	RESRAD-RECYCLE	MicroShield®
Development & Updates	Under Development (in progress code)	Last updated in 2005; (no official download available)	Periodically updated
Dose Analysis Approach	Exposure Scenario Evaluation (Single run for built-in scenarios)	Exposure Scenario Evaluation (Single run for built-in scenarios)	Object-based Evaluation (Multiple calculations for custom geometry)
External Dose Assessment	Point-kernel method	DCF fitting approach	Point-kernel method
Source Geometry	Various Geometries	Cylindrical Geometries	Various Geometries
External Dose Accuracy	Comparable accuracy to MicroShield®	Underestimation	Verified
Internal Dose Assessment	Supported	Supported	Not Supported
Suitability for Waste Recycling	Highly Suitable	Lack of Accuracy	Lack of Efficiency

benchmarks, such as annular cylinder and half-sphere. Because MS cannot assess these source geometries, other software tools capable of complex calculations, such as VISIPLAN 3D ALARA and MCNP codes [21,49], should be considered for additional comparisons. Existing studies noting differences between MCNP and other methodologies [50, 51] suggest that a comparison between RUCAS and MCNP could further verify the validity and conservatism of RUCAS. This approach will bolster the credibility of RUCAS and enhance its development into a robust radioactive waste management tool.

6. Conclusion

This study introduced and validated RUCAS, a new tool designed to assess the risks associated with recycling radioactive scrap metals generated from the decommissioning of nuclear facilities. RUCAS represents a significant advancement over existing tools, particularly in its refined algorithms for calculating exposure doses across various source geometries and shielding scenarios. The accuracy of RUCAS in evaluating both external and internal exposure doses across diverse recycling scenarios was validated, showcasing its superior precision and operational speed compared to tools such as RESRAD-RECYCLE and MS. RUCAS is a promising tool for assessing the radiological risks posed to radioactive waste recycling-operation workers and customers using recycled-content products. Using RUCAS to ensure the safety of recycled products could enhance public acceptance of radioactive scrap metal recycling, leading to more efficient use of disposal sites for radioactive waste and reduced decommissioning costs, as recycling can alleviate the burden on waste management facilities. Therefore, further validation of RUCAS is necessary. This is crucial to ensure reliable risk management in recycling radioactive waste.

CRediT authorship contribution statement

Ugyu Jeong: Writing – original draft, Visualization, Validation, Software, Methodology, Investigation. **Hyeongjin Byeon:** Writing – review & editing, Visualization, Data curation. **Jaeyeong Park:** Writing – original draft, Supervision, Project administration, Funding acquisition, Conceptualization.

Data availability

The data and software supporting the findings of this study are available from Korea Hydro & Nuclear Power Co. The data and software used under license for this study are not publicly available owing to restrictions.

Declaration of competing interest

The authors declare the following financial interests/personal relationships which may be considered as potential competing interests: Jaeyeong Park reports financial support was provided by Korea Hydro and Nuclear Power Co Ltd. If there are other authors, they declare that they have no known competing financial interests or personal relationships that could have appeared to influence the work reported in this paper.

Acknowledgments

This work was supported by KOREA HYDRO & NUCLEAR POWER CO., LTD. (No. 2020-Tech-13 and No. 2023-Tech-14).

References

[1] H.-W. Seo, D.-H. Lee, D.S. Kessel, C.-L. Kim, Proposal for the management strategy of metallic waste from the decommissioning of Kori Unit 1 by using melting and segmentation technology, Ann. Nucl. Energy 110 (2017) 633–647, https://doi.org/10.1016/j.anucene.2017.06.056.

[2] T. Hrncir, R. Strazovec, M. Zachar, Potential for recycling of slightly radioactive metals arising from decommissioning within nuclear sector in Slovakia, J. Environ. Radioact. 196 (2019) 212–224, https://doi.org/10.1016/j.jenvrad.2017.08.011.

[3] V. Remeikis, J. Grineviciute, G. Duškesas, L. Juodis, R. Plukienė, A. Plukis, Review of modeling experience during operation and decommissioning of RBMK-1500 reactors. II. Radioactive waste management, Nucl. Eng. Des. 380 (2021) 111242, https://doi.org/10.1016/j.nucengdes.2021.111242.

[4] Y.-J. Lim, B.-S. Lee, S.-O. Park, S.-G. Lee, A study on the clearance waste recycling scenario in the decommissioning of Korea's nuclear power plants, Ann. Nucl. Energy 178 (2022) 109366, https://doi.org/10.1016/j.anucene.2022.109366.

[5] I.G. Chang, J.H. Cheong, A new proposal for controlled recycling of decommissioning concrete waste as part of engineered barriers of a radioactive waste repository and related comprehensive safety assessment, Nucl. Eng. Technol. 55 (2023) 530–545, https://doi.org/10.1016/j.net.2022.10.028.

[6] B.-M. Jun, S.H. Chae, D. Kim, J.-Y. Jung, T.-J. Kim, S.-N. Nam, Y. Yoon, C. Park, H. Rho, Adsorption of uranyl ion on hexagonal boron nitride for remediation of real U-contaminated soil and its interpretation using random forest, J. Hazard Mater. 469 (2024) 134072, https://doi.org/10.1016/j.jhazmat.2024.134072.

[7] IAEA (International Atomic Energy Agency), Nuclear Power Reactors in the World, vol. 2, IAEA Reference Data Series No., 2023.

[8] IAEA (International Atomic Energy Agency), Managing Low Radioactivity Material from the Decommissioning of Nuclear Facilities, 2008. IAEA Technical Reports Series No. 462.

[9] A. Crégut, J. Roger, Inventory of Information for the Identification of Guiding Principles in the Decommissioning of Nuclear Installations, Commission of the European Communities, 1991, pp. EUR–13642.

[10] IAEA (International Atomic Energy Agency), Radiation Protection and Safety of Radiation Sources: International Basic Safety Standards, vol. 3, IAEA General Safety Requirements part, 2014.

[11] IAEA (International Atomic Energy Agency), Application of exemption principles to the recycle and reuse of materials from nuclear facilities, IAEA Saf. Ser. (111–P-1.1) (1992).

[12] A. Deckert, Basis for the definition of surface contamination clearance levels for the recycling or reuse of metals arising from the dismantling of nuclear installations, Radiat. Prot. European Commission. 101 (1998).

[13] S.F. Mobbs, M.P. Harvey, Methodology and Models Used to Calculate Individual and Collective Doses from the Recycling of Metals from the Dismantling of Nuclear Installations, European Commission, 2000. Final Report: Contract No 94-ET-009.

[14] R. Anigstein, H.J. Chmelynski, D.A. Loomis, S.F. Marschke, J.J. Mauro, R. H. Olsher, W.C. Thurber, R.A. Meck, Radiological Assessment for Clearance of Materials from Nuclear Facilities, NUREG-1640, United States Nuclear Regulatory Commission, Washington, District of Columbia, 2003.

[15] J.-J. Cheng, B. Kassas, C. Yu, D. Lepoire, J. Arnish, E.S. Dovel, S.-Y. Chen, W. A. Williams, A. Wallo, H. Peterson, RESRAD-recycle: a computer model for analyzing the radiological doses and risks resulting from the recycling of radioactive scrap metal and the reuse of surface. Contaminated Material and Equipment, No. ANL/EAD-3, Argonne National Laboratory, Argonne, Illinois, 2001.

[16] K.F. Eckerman, A.B. Wolbarst, A.C. Richardson, Limiting Values of Radionuclide Intake and Air Concentration and Dose Conversion Factors for Inhalation, Submersion, and Ingestion, Federal Guidance Report No. 11, Oak Ridge National Laboratory, Oak Ridge, Tennessee, 1988.

[17] K.F. Eckerman, J.C. Ryman, External exposure to radionuclides in air, water and soil. Federal Guidance Report No. 12, Oak Ridge National Laboratory, Oak Ridge, Tennessee, 1993.

[18] S. Kamboj, D. LePoire, C. Yu, External exposure model in the RESRAD computer code, Health Phys. 82 (2002) 831–839, https://doi.org/10.1097/00004032-200206000-00011.

[19] T. Hrncir, M. Panik, F. Ondra, V. Necas, The impact of radioactive steel recycling on the public and professionals, J. Hazard Mater. 254–255 (2013) 98–106, https://doi.org/10.1016/j.jhazmat.2013.03.038.

[20] Grove Software Inc, MicroShield® user's manual. https://radiationsoftware.com/. (Accessed 22 April 2024).

[21] F. Vermeersch, VISIPLAN, 3D ALARA Planning Tool, User's Guide, SCK Cen, 2005.

[22] P.C. Jackson, Age-dependent doses to members of the public from intake of radionuclides: part 5 Compilation of ingestion and inhalation dose coefficients (ICRP Publication 72), Phys. Med. Biol. 41 (1996) 2807, https://doi.org/10.1088/0031-9155/41/12/017.

[23] K. Eckerman, A. Endo, ICRP, ICRP Publication 107, Nuclear decay data for dosimetric calculations, Ann. ICRP 38 (2008) 7–96, https://doi.org/10.1016/j.icrp.2008.10.004.

[24] N. Petoussi-Henss, W.E. Bolch, K.F. Eckerman, A. Endo, N. Hertel, J. Hunt, M. Pelliccioni, H. Schlattl, M. Zankl, Conversion coefficients for radiological protection quantities for external radiation exposures, Ann. ICRP 40 (2010) 1–257, https://doi.org/10.1016/j.icrp.2011.10.001.

[25] H. Bateman, The solution of a system of differential equations occurring in the theory of radioactive transformations, Proc. Camb. Phil. Soc. 15 (1910) 423–427, https://doi.org/10.1093/ww/9780199540884.013.u176787.

[26] R.G. Jaeger, Engineering Compendium on Radiation Shielding: Volume I: Shielding Fundamentals and Methods, Springer Science & Business Media, 2013.

[27] R.L. Iman, M.J. Shortencarier, FORTRAN 77 Program and User's Guide for the Generation of Latin Hypercube and Random Samples for Use with Computer Models (No. NUREG/CR-3624; SAND-83-2365), Sandia National Laboratories (SNL-NM), Albuquerque, New Mexico, 1984.

[28] IAEA (International Atomic Energy Agency), Derivation of Activity Concentration Values for Exclusion, Exemption and Clearance, IAEA, 2005. Safety Report Series No. 44.
[29] ICRP (International Commission on Radiological Protection), Data for Use in Protection against External Radiation, vol. 51, International Commission on Radiological Protection, 1987. ICRP Publication.
[30] ICRP (International Commission on Radiological Protection), Radionuclide Transformations - Energy and Intensity of Emissions, vol. 38, International Commission on Radiological Protection, 1983. ICRP Publication.
[31] ANS (American Nuclear Society), Gamma-ray Attenuation Coefficients and Buildup Factors for Engineering Materials, ANSI/ANS-6.4.3-1991, American Nuclear Society, 1991.
[32] Y. Harima, An approximation of gamma-ray buildup factors by modified geometrical progression, Nucl. Sci. Eng. 83 (1983) 299–309, https://doi.org/10.13182/NSE83-A18222.
[33] M.H. Kalos, A Monte Carlo Calculation of the Transport of Gamma Rays (No. NDA-56-7), Nuclear Development Corporation of America, 1956.
[34] U.T. Lin, S.H. Jiang, A dedicated empirical formula for γ-ray buildup factors for a point isotropic source in stratified shields, Radiat. Phys. Chem. 48 (1996) 389–401, https://doi.org/10.1016/0969-806X(95)00461-6.
[35] S. Menon, C. Brun-Yaba, C. Yu, J.-J. Cheng, J. Bjerler, A. Williams, Validation of dose calculation programmes for recycling (No. SSI–2002-23), Swedish Radiation Protection Authority (2002).
[36] M. Sappok, Results of melting large quantities of radioactive steel scrap, Nucl. Technol. 86 (1989) 188–191, https://doi.org/10.13182/NT89-A34269.
[37] M. Elert, M. Wiborgh, A. Bengtsson, Basis for Criteria for Exemption of Decommissioning Waste (No. KEMAKTA-AR-98-08, Swedish Radiation Protection Institute, 1992.
[38] A.M. Chapuis, P. Guetat, H. Garbay, Exemption limits for the recycling of materials from the dismantling of nuclear installations, in: International Decommissioning Symposium, 1987.
[39] IAEA (International Atomic Energy Agency), Radiological Characterization of Shut Down Nuclear Reactors for Decommissioning Purposes, IAEA, 1998. Technical Reports Series No. 389.
[40] L.A. Bowman, Monte Carlo calculation of gamma-ray dose-rate buildup factors for lead and water shields and Monte Carlo calculation of the deposition of gamma-ray heating, in: Stratified Lead and Water Slabs, Oak Ridge National Laboratory, Oak Ridge, Tennessee, 1958. ORNL-2609.
[41] D.L. Broder, Y.P. Kayurin, A.A. Kutuzov, Transmission of gamma radiation through heterogeneous media, Energy 12 (1962) 26–31, https://doi.org/10.1007/BF01475996.
[42] S.-I. Miyasaka, A. Tsuruo, Dose buildup factors of multi-layer slabs for a point isotropic source, J. Nucl. Sci. Technol. 3 (1966) 393–400, https://doi.org/10.3327/jnst.3.393.
[43] G.P. Burke, H.L. Beck, Calculated and measured dose buildup factors for gamma rays penetrating multilayered slabs, Nucl. Sci. Eng. 53 (1974) 109–112, https://doi.org/10.13182/NSE74-A23334.
[44] P. Basu, R. Sarangapani, B. Venkatraman, An improvement to the Kalos' formula for double layer gamma ray exposure buildup factors for shielding materials of nuclear and radiological facilities, Ann. Nucl. Energy 151 (2021) 107944, https://doi.org/10.1016/j.anucene.2020.107944.
[45] I.I. Bashter, Calculation of radiation attenuation coefficients for shielding concretes, Ann. Nucl. Energy 24 (1997) 1389–1401, https://doi.org/10.1016/S0306-4549(97)00003-0.
[46] I. Akkurt, R. Altindag, K. Gunoglu, H. Sarıkaya, Photon attenuation coefficients of concrete including marble aggregates, Ann. Nucl. Energy 43 (2012) 56–60, https://doi.org/10.1016/j.anucene.2011.12.031.
[47] T.A. Almeida Junior, M.S. Nogueira, V. Vivolo, M.P.A. Potiens, L.L. Campos, Mass attenuation coefficients of X-rays in different barite concrete used in radiation protection as shielding against ionizing radiation, Radiat. Phys. Chem. 140 (2017) 349–354, https://doi.org/10.1016/j.radphyschem.2017.02.054.
[48] M.J. Berger, J.H. Hubbell, S.M. Seltzer, J. Chang, J.S. Coursey, R. Sukumar, D. S. Zucker, K. Olson, XCOM: Photon Cross Sections Database, National Institute of Standards and Technology, 1998.
[49] J.F. Briesmeister, MCNP-A general Monte Carlo N-particli transport code, LA-12625-M (1993).
[50] D. Bednár, M. Ličtjak, A. Slimák, V. Nečas, Comparison of MCNP and VISIPLAN dose-field calculations for multilayer shielding, Radiat. Protect. Dosim. 186 (2019) 310–314, https://doi.org/10.1093/rpd/ncz224.
[51] B.M. Mendes, P.C.G. Antunes, I.S.L. Branco, E. do Nascimento, B. Seniwal, T.C. F. Fonseca, H. Yoriyaz, Calculation of dose point kernel values for monoenergetic electrons and beta emitting radionuclides: intercomparison of Monte Carlo codes, Radiat. Phys. Chem. 181 (2021) 109327, https://doi.org/10.1016/j.radphyschem.2020.109327.